

# ON THE PERFORMANCE OF COMPRESSOR BLADES WITH CONTOURED ENDWALLS

M. Hoeger \*      N. Sievers and M. Lawerenz \*\*

\* MTU Aero Engines, Compressor Department, Munich , Germany  
Martin.Hoeger@muc.mtu.dasa.de

\*\* Institut für thermische Energietechnik, University of Kassel, Kassel, Germany  
lawerenz@ite.maschinenbau.uni-kassel.de and  
nsievers@student.uni-kassel.de

## ABSTRACT

To investigate endwall flows at engine-like loading levels and Mach numbers a plane compressor cascade with linear contracting end wall sections was designed. The profile type is comparable to a typical rotor root section. In a second step endwall shapes from actual engines and the open literature are examined. An optimum endwall shape is designed to improve the cascade. Investigations are performed at 3 levels of complexity: (1) Design level S1/ S2, (2) S2 meridional Navier-Stokes and (3) 3D Navier-Stokes code *TRACE\_S*.

The impact of the contour shape on the flow behaviour is discussed in terms of loss, secondary flow and endwall boundary layer thickness. On the basis of 3D Navier-Stokes predictions a concave contour shape is successfully demonstrated to reduce blade loading but to increase pre-shock Mach numbers. A new non-axis symmetric endwall contour is presented, which allows the reduction of blade loading without any shock-loss penalties.

## INTRODUCTION

In the first stages of today's advanced compressor components high loading levels and corrected tip speeds are found. For the rotor root sections, where small pitch to chord ratios coincide with a relatively high thickness to chord ratios and high flow turnings, undesirable overspeeds occur which increase losses and reduce stall margin. Here end wall contouring is applied to nearly all civil and military fan stages, see [Fig. 1](#). An example for successfully controlling hub corner separation for a HPC rotor is given by *LeJambre* et al. in [1]. For a concave hub shape the open flow area is increased, allowing it to compensate for overspeeds from high thickness and excessive suction surface curvature in the rear part of the blade. Similar findings are reported by *Stringham* et al. [2] for an industrial gasturbine with contoured rotor hub sections down to the 9<sup>th</sup> stage.

Several authors investigate the impact of hub contouring on endwall flow in turbine configurations, see e.g. [3]. For transonic compressor cascades only some work is published for highly loaded, high turning compressor cascades in 2D flow, see e.g. [4], but no detailed investigations exist dealing with hub contouring. Patents for contoured endwalls are given by *Matthewes* et al. [5] in 1987, *Spear* et al. [6] in 1995 and *Hoeger and Schmidt-Eisenlohr* [7] in 1998.

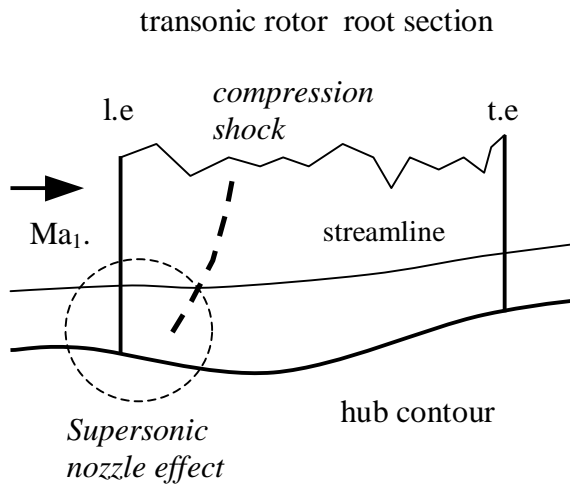


Fig. 1: Increased pre-shock Mach number for concave shaped hub contour

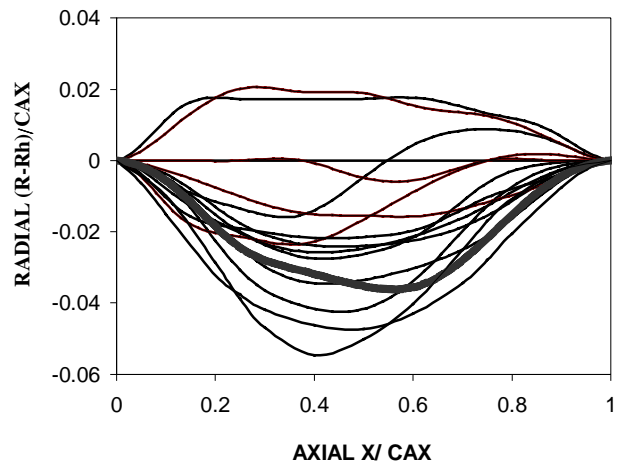


Fig. 2: Hub contour shapes from engines in service and out of literature

### Existing Hub Contours

Typical hub contour shapes in the meridional plane for 5 fan configurations and 10 HPC front stages are given in Fig. 2 as radial departure from a hypothetical linear hub contour between leading and trailing edge. Although some data which were taken directly from drawings out of the literature may be of limited accuracy, a clear trend towards concave hub shapes is observed. The maximum depth of the contours considered does not exceed a value of 6 % of the axial chord,  $cax$ . Four classes of contour shapes may be distinguished in Fig. 2: convex, linear, concave-convex in the rear and solely concave. A concave hub shape with convex parts at the leading- and the trailing edge is subject to the patent [6].

### Background and Motivation

Especially for the front stages of highly loaded HP-compressors and stationary gasturbines as well as for high speed boosters relative inlet Mach numbers close to  $Ma_1 = 0.9$  may occur at the rotor root sections at off-design. In this situation the control of endwall flow is imperative to ensure stable and dependable operation of the compression system without severe efficiency penalties. Looking on the results of [1] the concave endwall shape is found to reduce the loading in the rear part of the root section while in the front part at transonic speeds a ‘supersonic nozzle’ effect is found, which promotes an undesirable increase in Mach number and shock strength, see diverging streamlines in Fig.1. In the following chapters the positive and negative aspects of a concave hub contour at transonic flow will be investigated more closely. A new non-axis symmetric endwall shape [7], [8] will be demonstrated to improve endwall flow at inlet Mach number levels  $Ma_1 = 0.85$ .

## **COMPRESSOR CASCADE INVESTIGATED**

To eliminate the influences of a skewed inlet profile and a non-uniform work distribution present in an actual rotor blade the investigations are performed for the relative flow quantities in a compressor cascade with contracting endwalls. Straight blades are designed first for a linear hub contour. The maximum permissible aerodynamic loading is defined from S1 predictions on the 12.5% mass flow reference streamline by a boundary layer close to separation. The reference streamline is situated at approximately 12.5%  $cax$  distance from the wall close to the location of the maximum underturning. With secondary flow included, the 3D simulations reveal a confined separation on the suction surface in the vicinity of the hub,

for separation criteria in corner flows see [9]. Design of the cascades is partly performed within the EC 5<sup>th</sup> Framework project ‘Advanced Compressor Blade Design’ *AdComB*. Experimental investigations of the cascade are planned at the University of the Armed Forces Munich High Speed Cascade Windtunnel.

### Cascade Geometry

The cascade consists of CDA profiles (Controlled Diffusion Airfoil). To achieve 2D inlet flow conditions the design was performed on a radius of 10 m (midsection) with a hub to tip ratio approaching unity. With the entrance section designed carefully the flow angle and Mach number spanwise non-uniformities were below 0.4 deg and 0.01 respectively outside the hub boundary layer. The geometric and aerodynamic parameters are given in Tab. 1.

<i>Geometry</i>		<i>Aerodynamic (ref. location at 12% halfspan)</i>	
thickness/ chord	$t/c = 0.095$	inlet Mach number	$Ma_1 = 0.85$
pitch/ chord	$s/c = 0.510$	ax velocity density ratio	$AVDR = 1.19$
stagger	$\beta_s = 22.4 \text{ deg}$	Reynolds number	$Re_1 = 0.9 \cdot 10^6$
aspect ratio (H/2)	$AR = 0.90$	2D turning	$\Delta\beta = 35 \text{ deg}$
profile type	CDA	diffusion factor	$Dr = 0.5$
with straight blades		displ. thickness at inlet	$\delta_1/c = 0.0079$
chord	$c = 0.14 \text{ m}$	de Haller No.	$v_2/v_1 = 0.67$

Tab. 1: Compressor cascade profile parameters

### Endwall Contour Optimisation Study

The hub contour is pre-defined using S2 through-flow and Q3D Euler-boundary layer codes by iteratively changing the depth of the concave contour as well as its maximum location. No optimiser was used at this stage of the investigations. An optimum contour was then chosen from a minimum shape parameter  $H = \delta_1/\theta$  ( $\delta_1$  displacement thickness,  $\theta$  momentum loss thickness) close to the trailing edge region. In a second step the contour was further refined by fully 3D Navier-Stokes predictions including now the influence of secondary flows on the optimum hub shape geometry.

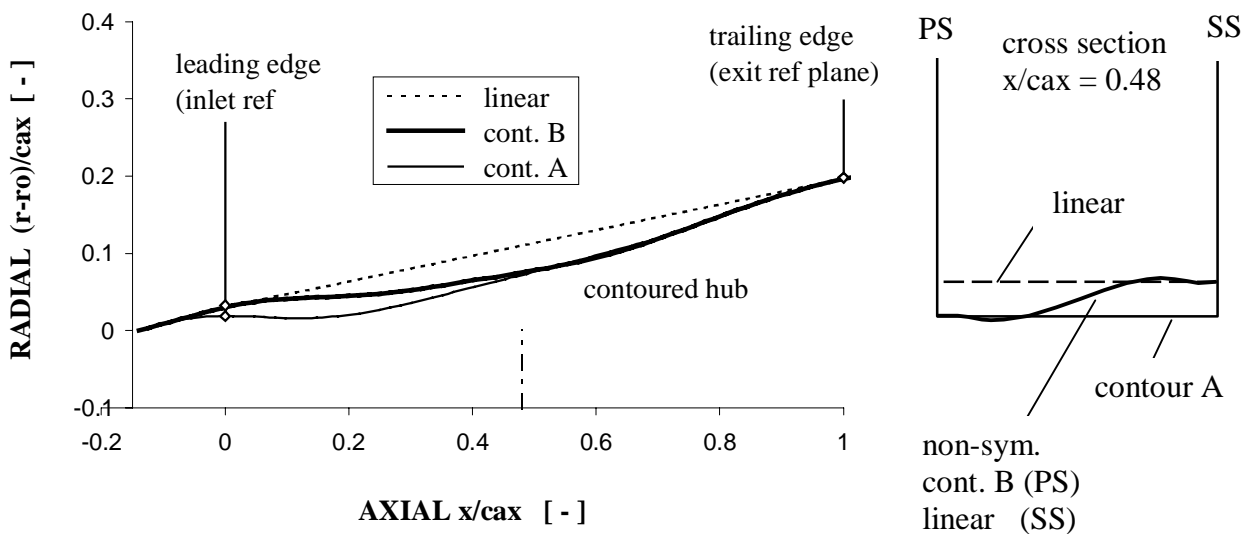


Fig. 3: Endwall contour shapes investigated (left side); cross section at  $x/cax = 0.48$  (right side)

### Endwall Shapes

From several endwall shapes investigated, 3 are presented in this paper, see Fig. 3.

- (1) linear
- (2) concave contoured, referred to as cont. A
- (3) non-axis symmetric contour, referred to as non-sym.

The non-axis symmetric contour is constructed with contour B on the pressure side and a linear hub shape on the suction side. A sine-type function was used to define the hub shape in pitch direction, see Fig. 3, right. A comparison of actual endwall shapes is made in fig. 2, where contour B is indicated by a bold line.

## **NUMERICAL SIMULATIONS**

From symmetry considerations the computational domain covered only one half of the passage. This doubles the number of grid lines in the spanwise direction compared to a standard turbomachine simulation. At midspan a symmetry boundary condition is applied.

### S1/ S2 Simulations

The design of the cascade blade was performed with an in-house through-flow method, which was run in the standard design mode with exit flow angle prescribed. The actual blade blockage as well as the pitch averaged flow angles from the 3D Navier-Stokes results were prescribed at 5 stations for the blade passage. The resulting streamsurface geometry was then input to a S1 Euler-boundary-layer method [10].

### S2 meridional Navier-Stokes

Code Details: The circumferentially averaged viscous equations [11] are solved by a partially parabolised procedure introduced by Pantankar [12]. The equations are transformed into a non-orthogonal co-ordinate system and viscous terms with derivatives in the streamwise direction are neglected. Upstream effects of the pressure field are taken into account by the use of an elliptic pressure correction which is based on the continuity equation. In order to predict the blade force, the momentum equation in the tangential direction is used inside the cascade to calculate the corresponding component. Radial and axial components of the inviscid blade force result from the condition that this force acts normal to the S2 stream surface. Additionally a viscous force is used which acts parallel to the velocity vector. This force is related to correlations for total pressure losses due to profile boundary layers, secondary flow and tip clearance vortices.

Calculations: The grid consists of 120x39 nodes in axial and spanwise direction respectively. Twenty nodes are located in the endwall boundary layer. The blockage of the blades is specified by the actual profile. The inlet flow conditions are chosen in a way, that design flow conditions are met at midspan. At the cascade inlet the displacement thickness of the endwall boundary layer was close to the design value given in Tab. 1. Inside the cascade the flow angle in the circumferential direction is calculated using a cubic distribution in order to approximate the pitch averaged 3D Navier-Stokes data.

### 3D Navier-Stokes

Details of the Navier-Stokes solver *TRACE\_S*, an explicit cell-centered 2<sup>nd</sup>-order-accurate finite-volume scheme, are given in [13]. Its extension to multistage and to parallel architectures are found in [14]. The code was widely validated to ensure all relevant phenomena are captured in principle [13], [15].

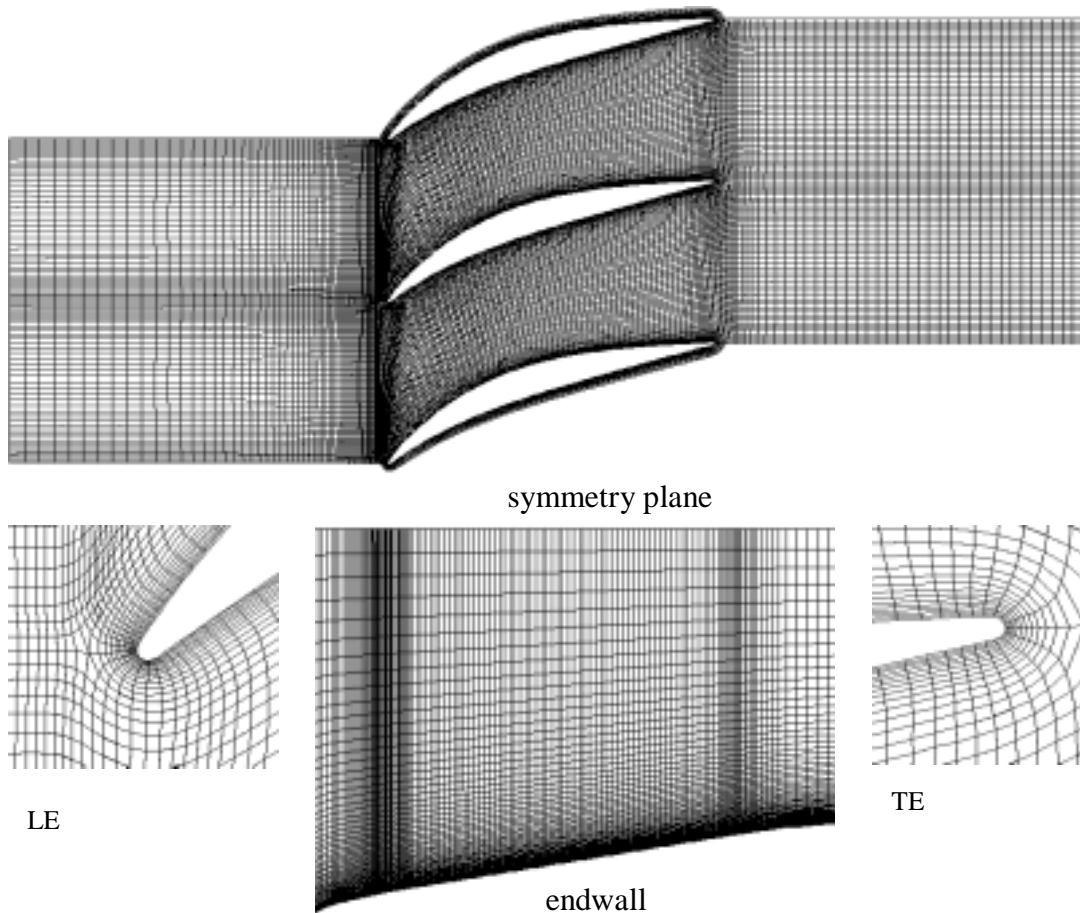


Fig. 4: Cascade blade with H/ O grid combination

**Grid Topology and CPU-Time:** Block-structured grids are employed to obtain high-quality grids and accurate convergent simulations for the complex geometry found in turbomachinery. All simulations utilised a composite H/O-grid with 181x41 nodes for the H-grid and 169x13 nodes for the O-grid in the S1-plane; 65 nodes were used in the radial direction, to yield a combined total of 719,394 nodes. A representation of the grid is given in Fig. 4. Extensive grid studies, partly documented in Fritsch et. al [13], were performed to ensure the results of the simulation not to be compromised by a lack of resolution. Execution time to convergence is approx. 37 CPU-hours on a *SGI-Origin 2000* with one R10\_250 processor.

**Turbulence Model:** For economy a high Reynolds'  $k-\epsilon$  model, resulting in a mean wall distance of  $y^+=15$  to 30 at the hub was used. All simulations were run in the fully turbulent mode with wall functions applied to accurately represent the wall shear. A turbulence level of 4% at the entrance to the blade passage was used.

**Calculations:** Boundary conditions at the inlet of the computational domain were prescribed in a way to achieve the desired flow angle and Mach number at 12.5 % cax distance from the endwall at cascade inlet plane,. The linear contour showed a fairly constant inlet angle, while under the influence of contour A a smooth variation of about 0.75 deg. occurred along the span. For all hub shapes homo-geneous inlet Mach number distributions

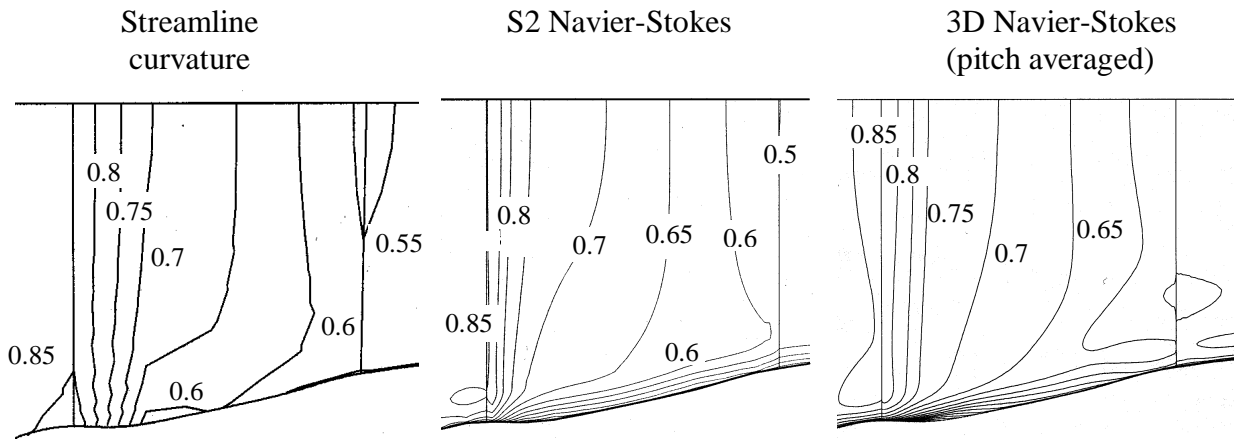


Fig. 5: Iso Mach surfaces in the meridional plane for endwall contour A; comparison of simulations with increasing level complexity

were observed outside the endwall boundary layer. The mass flow variations were below 0.2 % for all 3 cases with a slightly higher mass flow for contour A.

## ANALYSIS OF RESULTS

In the following chapters only design conditions are considered.

### Simulations with Varying Level of Complexity

A large area of decelerated flow is predicted by the through-flow method at the concave hub region, [Fig. 5, left](#). Smoothing of the effective endwall shape is observed for the meridional Navier-Stokes results with the hub boundary layer included., [Fig. 5, mid](#). The averaged 3D Navier-Stokes predictions are in close agreement with the S2 Navier-Stokes solution in the front parts of the blade passage, see [Fig 5, right](#). In the rear part of the passage convective loss transport from the endwall to the suction side of the blade is visible for the 3D Navier-Stokes results, see low Mach number region  $Ma = 0.55$  close to the trailing edge in [Fig. 5, right](#). This flow feature is not captured by the meridional approach directly but may be modelled in the loss correlations used in the through-flow and the S2-Navier-Stokes method.

The present results indicate the meridional Navier-Stokes approach to be capable to resolve the endwall boundary layer in the front part of the cascade in principle. While the S2-codes offer the advantage of a rapid optimisation, their dependency on loss modelling led the authors to continue the analysis of endwall contour effects on a 3D Navier-Stokes level.

### 3D Navier-Stokes Results

Conservative variables of the momentum equations are used to obtain pitchwise averaged flow quantities from the 3D Navier-Stokes results. Local as well as average values are interpolated on streamsurfaces in the meridional plane to enable an adequate comparison of results for different geometries.

Adiabatic Mach number distributions: In [Fig. 6](#) Iso Mach surfaces are given in an axial plane at midchord  $x/cax = 0.48$ . With contour A the highest Mach number reduction of 0.05 is found. For the non-axis symmetric contour still about half the Mach number reduction occurs on the suction side compared to contour A. Endwall contouring influence is not only

confined to the hub region but extends to the mid section, see  $Ma_{is} = 0.75$  in Fig. 6. This may become important for rotors where Mach number and shock strength increases with span.

**Profile Mach number distribution:** The isentropic Mach numbers on the reference streamline are given in Fig. 7. For an unchanged profile geometry, contour A shows a beneficial loading decrease in the rear part of the profile. Close to the leading edge a supersonic expansion arises on the suction surface as a consequence of the diverging streamlines, see Fig. 1. The pre-shock Mach number increases from 1.15 for the linear- to 1.25 for contour A and the shock type changes from supercritical to a normal shock. With the non-axis symmetric contour the supersonic part of the flow field remains unchanged, with a moderate unloading in the rear part of the suction surface. It is worth noting that other contour shapes, e.g. symmetrical contour B led to similar pre-shock Mach numbers like contour A.

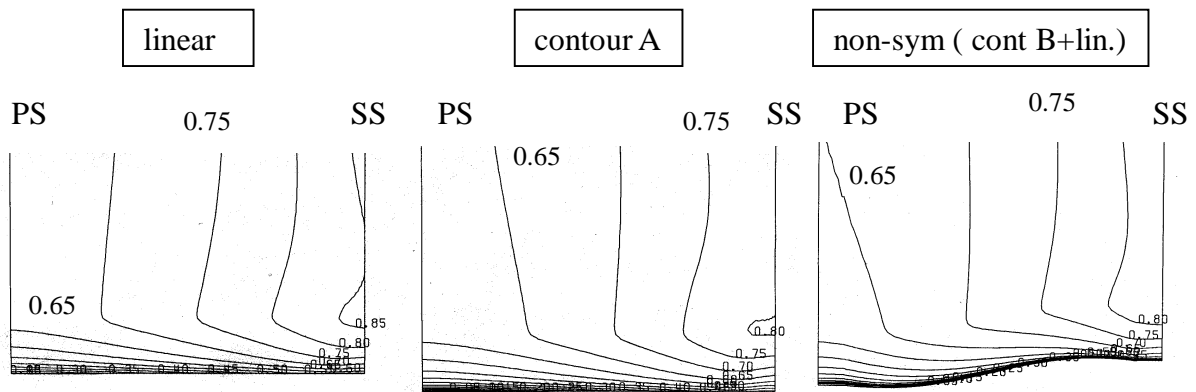


Fig. 6: Isentropic Mach number contours at midchord axial plane  $x/c_{ax} = 0.48$ ; boundary layer like Iso lines at hub from specified inlet total pressure profile

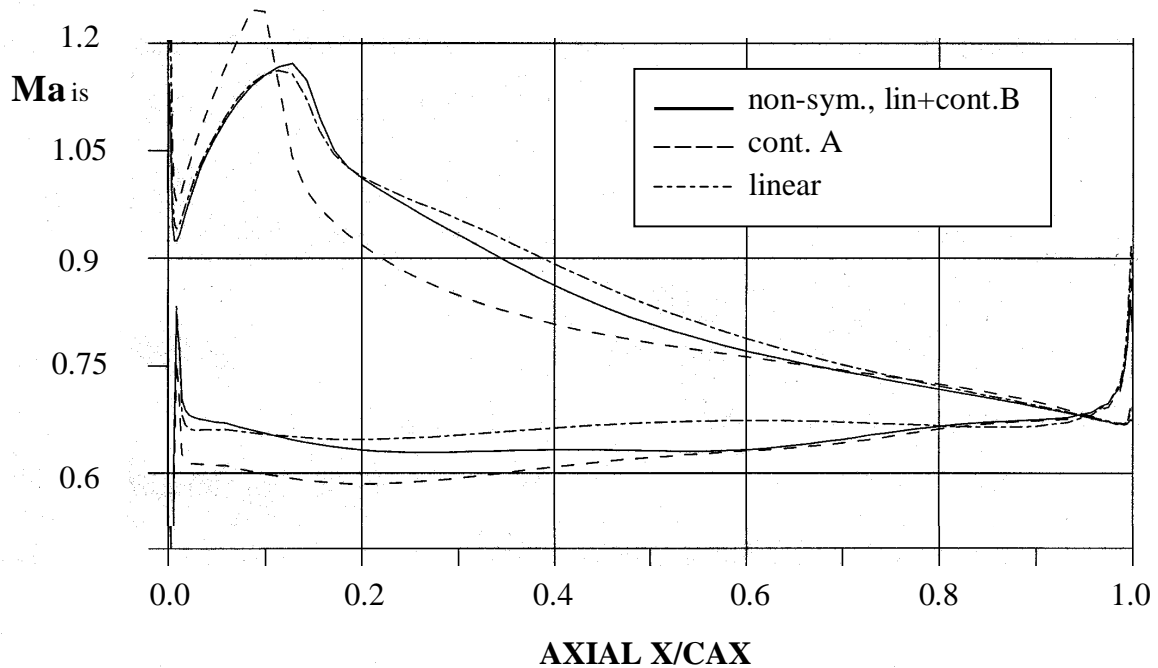


Fig. 7: Profile section isentropic Mach numbers (12.5% mass flow reference streamline); influence of endwall contouring for unchanged blade shape

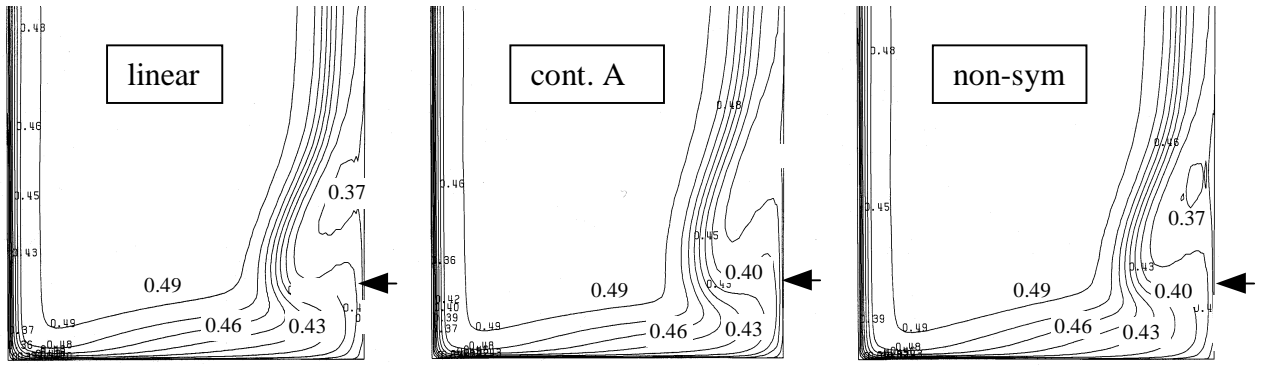


Fig. 8: Total pressure contours in the trailing edge plane (increment 0.015);  
reduced 3D separation from hub contouring (ref. position indicated by arrow)

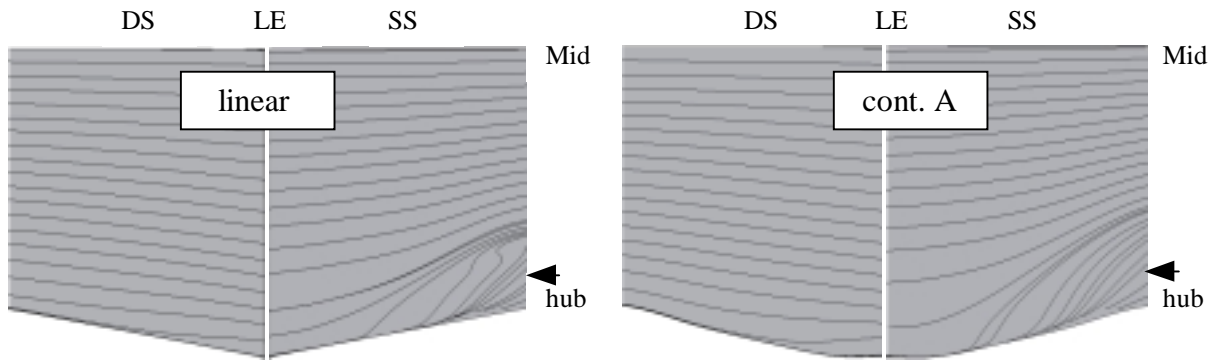


Fig. 9: Streamlines on pressure and suction surface;  
3D separation on SS for linear hub shape (ref. position indicated by arrow)

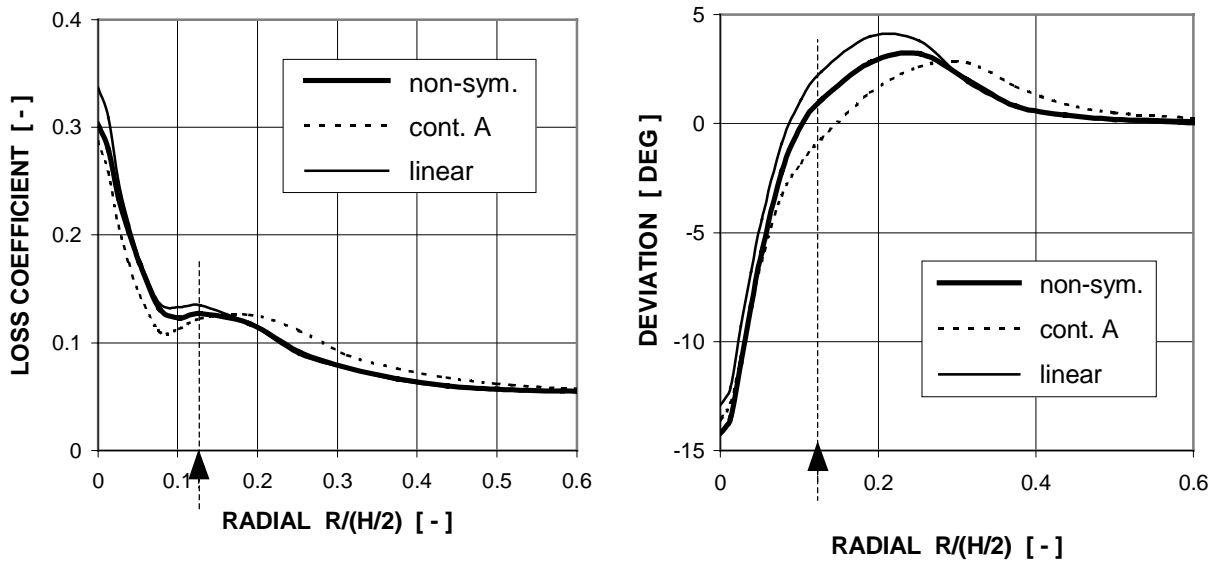


Fig. 10: Spanwise distribution of loss coefficient and exit flow angle deviation;  
(ref. position indicated by arrow, rel. radial co-ordinate with half passage height ( $H/2$ ))

### Loss Mechanisms and Deviation

Losses: The total pressure surfaces in [Fig. 8](#) clearly reveal a characteristic separation zone, where low energy material is driven via the passage vortex to the suction surface forming a complex 3D boundary layer separation, see [Fig. 9](#). Here the unloading by contour A reduces the maximum total pressure defect most. Pitch averaged loss coefficients are given in [Fig. 10, left](#) for the 3 cascade configurations. For contour A a clear reduction in loss close to the wall is accompanied by a loss increase originating from the higher pre-shock Mach numbers in some distance to the endwall outside the boundary layer. A 1% higher mass-averaged total loss coefficient is obtained compared to the linear case. With the non-axis symmetric contour all along the span a moderate improvement is achieved resulting in an approx. 2% lower loss coefficient. Up to now only 3 non-axis symmetric configuration have been examined and further improvement potential is expected from a refined hub shape at the suction surface. With spanwise increasing Mach numbers for an actual compressor rotor and a 5% higher loading potential in the region between hub and midspan for the non-axis symmetric contour rotor efficiency benefits in the order of 0.5% are estimated.

Deviation: With the reduction of the separation zone on the suction side the maximum underturning is reduced too, see [Fig. 10, right](#). In addition, for contour A the location of the maximum underturning is shifted towards higher wall distances.

### **SUMMARY AND CONCLUSIONS**

A compressor cascade has been designed to numerically study the impact of endwall contouring on the aerodynamic behaviour of a typical rotor root section profile at transonic flow conditions. Flow simulations are performed on three levels of complexity: (1) S2 through flow- and S1 method, (2) meridional Navier-Stokes- and (3) 3D Navier-Stokes code.

On the basis of 3D Navier-Stokes simulations three endwall contours linear, concave and non-axis symmetric are investigated for unchanged blade shape. Compared to the linear shape the concave contour demonstrates considerable loading reduction potential in the rear part of the profile close to the hub. This beneficial influence was not confined to the hub region but extended all along the span up to the mid section.

In the front part higher mass flows and higher pre-shock Mach numbers result from the increase in flow area which leads to an undesirable acceleration similar to the flow in a supersonic nozzle. Hereby the losses increase in some wall distance outside the endwall boundary layer and the location of the maximum underturning moves to higher wall distances. A new non-axis symmetric endwall contour shape is introduced, which combines a concave contour at the pressure side with a linear endwall shape close to the suction side. By that a favourable unloading of the suction side profile boundary layer is achieved without any increase in shock strength and losses.

While standard concave endwall contours may be used at subsonic flow conditions, the non-axis symmetric contour shape allows a further advance in flow capacity and efficiency levels of highly loaded LPC and HPC front stages at reduced component weights. Especially for high relative inlet Mach numbers at the hub the use of non-axis symmetric contouring may enable efficiency benefits in the order of 0.5% from shock loss reduction.

## ACKNOWLEDGEMENTS

The support of parts of the present design study through the European Commission within the ‘Advanced 3D Compressor Blade Design’ project, AdComB, under Contract No, GRAD-CT-2000-0007 (SCO R.Simonini) is gratefully acknowledged. The authors further would like to thank B. Stubert of MTU Aero Engines for his support in gridding complex geometries.

## REFERENCES

- [1] LeJambre, C.R., Zacharias, R.M., Biederman, B.P., Gleixner, A.J., Yetka, C.J. (1996). Development and Application of a Multistage Navier-Stokes Solver - Part II: Application to a High Pressure Compressor Design. ASME Paper 95-GT-343.
- [2] Stringham, G.D., Cassem, B.N., Prince, T.C., Yeung, P.F. (1998). *Design and development of a nine stage axial flow compressor for industrial gas turbines*. ASME-Paper 98-GT-140.
- [3] Duden, A. (1999). *Strömungsbeeinflussung zur Reduzierung der Sekundärströmungen in Turbinengittern*. Shaker Verlag Aachen.
- [4] Hoheisel, H., Seyb, N.J. (1986). *The boundary layer behaviour in a highly loaded compressor cascade at transonic flow conditions*. AGARD CPP-400/401 68<sup>th</sup> Specialists Meeting, Munich, Germany.
- [5] Matthews, J:A. et al.(1987). *Circumferentially Area Ruled Duct*. United States Patent No. 4.677.828.
- [6] Spear, D. A., Biedermann, B.P. (1995). *Flow Directing Assembly for the Compression Section of a Rotary Machine*. United States Patent – No. 5.397.215.
- [7] Hoeger, M., Schmidt-Eisenlohr, U. (1998). *Turbomaschine mit transsonischer Verdichterstufe*. European Patent Office Patent No. EP 0846867.
- [8] Hoeger, M., Schmidt-Eisenlohr, U. (2000). *Rotary Turbomachine having a transonic compressor stage*. United States Patent No. 6017186.
- [9] Scheugenpflug H. (1990). *Theoretische und experimentelle Untersuchungen zur Reduzierung der Randverluste hochbelasteter Axialverdichter durch Grenzschichtbeeinflussung*. Dissertation Institut für Strahlantriebe, Uni BW München.
- [10] Hoeger, M., Broichhausen, K.D. (1992). *Prediction of 2D Viscous Transonic Flow in Compressor Cascades Using a Semi-Empirical Shock/Boundary-Layer Interaction Methods*. ASME Paper 92-GT-277.
- [11] Fay, G., Lawrenz, M. and Przewozny, H. (1999). *Calculations of pitch averaged viscous flow in an annular compressor cascade*. In: Carlomagno G.M. and Brebbia C.A. editors. Computational Methods and Experimental Measurements IX. Witpress.
- [12] Pantankar, S.W. and Spalding, D.W. (1972). *A calculation procedure for heat, mass and momentum transfer in three-dimensional parabolic flows*. Int. J. Heat and Mass Transfer, 15.
- [13] Fritsch, G., Hoeger, M., Blaha, C., Bauer, D. (1997). *Viscous 3D Compressor Simulation on Parallel Architectures*. AIAA 97-2876.
- [14] Fritsch, G., Möhres, W. (1997). *Multistage Simulations for Turbomachinery Design on Parallel Architectures*. Proc. of Parallel Computational Fluid Dynamics Conf., Elsevier Science, Amsterdam, 1997, pp. 225-238.
- [15] Hoeger, M., Fritsch, G., Bauer, D. (1998). *Numerical Simulation of the Shock-Tip Leakage Vortex Interaction in a HPC Front Stage*. ASME-Paper 98-GT-261.